Title

Obesity induces gut microbiota alterations and augments acute graft-versus-host disease after allogeneic stem cell transplantation

Journal

Science Translational Medicine, 12(571)

ISSN

1946-6234

Authors

Khuat, Lam T

Le, Catherine T

Pai, Chien-Chun Steven

et al.

Publication Date

2020-11-25

DOI

10.1126/scitranslmed.aay7713

Peer reviewed

HHS Public Access

Author manuscript

Sci Transl Med. Author manuscript; available in PMC 2021 November 25.

Published in final edited form as:

Sci Transl Med. 2020 November 25; 12(571): . doi:10.1126/scitranslmed.aay7713.

Obesity Induces Gut Microbiota Alterations and Augments Acute Graft-Versus-Host Disease After Allogeneic Stem Cell Transplantation

Lam T. Khuat[1], **Catherine T. Le**[1], **Chien-Chun Steven Pai**[1], **Robin R. Shields-Cutler**[2], **Shernan G. Holtan**[3], **Armin Rashidi**[3], **Sarah L. Parker**[4], **Dan Knights**[5], **Jesus I. Luna**[1], **Cordelia Dunai**[1], **Ziming Wang**[1], **Ian R. Sturgill**[1], **Kevin Stoffel**[1], **Alexander A. Merleev**[1], **Shyam K. More**[6], **Emanual Maverakis**[1], **Helen Raybould**[7], **Mingyi Chen**[8], **Robert J. Canter**[9], **Arta M. Monjazeb**[10], **Maneesh Dave**[6], **James L. M. Ferrara**[11], **John E. Levine**[11], **Dan L. Longo**[12], **Mehrdad Abedi**[13], **Bruce R. Blazar**[14], **William J. Murphy**[1,13,*]

[1]Department of Dermatology, School of Medicine, University of California, Davis, CA, United States, 95817

[2]Department of Biology, Macalester College, Saint Paul, MN, United States, 55105

[3]Blood and Marrow Transplant Program, University of Minnesota, Minneapolis, MN, United States, 55455

[4]Department of Internal Medicine, University of Minnesota, Minneapolis, MN, United States, 55455

[5]Department of Computer Science and Engineering, BioTechnology Institute, University of Minnesota, Minneapolis, MN, United States, 55455

[6]Division of Gastroenterology, Department of Internal Medicine, School of Medicine, University of California, Davis, CA, United States, 95817

[7]Department of Anatomy, Physiology and Cell Biology, School of Veterinary Medicine, University of California, Davis, CA, United States, 95616

[8]Department of Pathology and Laboratory Medicine, UT Southwestern Medical Center, Dallas, TX, United States, 75390

[*]**Corresponding author:** William J. Murphy, Ph.D., wmjmurphy@ucdavis.edu.

Current Institutional Affiliation of I.R.S: University of North Carolina at Chapel Hill (as a Graduate Research Assistant).

Current Affiliation of C-C.S.P.: Department of Oncology Biomarker Development, Genentech, South San Francisco, CA, United States

AUTHOR CONTRIBUTIONS

L.T.K, C.T.L., C-C.S.P., C.D., Z.W., K.S., S.K.M performed studies in B10.D2→BALB/c + SC model. L.T.K, C.T.L., C.D. performed studies in B10.D2→BALB/c + CD4 and B10.D2→BALB/c + CD8 models. L.T.K, C.T.L., C-C.S.P., C.D., Z.W., K.S. performed studies in BALB/c→C57BL/6 + T model. L.T.K, C.T.L., C.D. performed studies in C3H.SW→C57BL/6 + CD8 model. L.T.K, C.T.L., C-C.S.P., J.I.L., C.D., Z.W., I.R.S., K.S., A.A.M., S.K.M., E.M., H.R., M.C., R.J.C., A.M.M., M.D., D.L.L., M.A., B.R.B., W.J.M. performed murine studies data analysis and interpretation. R.R.S-C., S.G.H., A.R., S.L.P., D.K., J.L.M.F., J.E.L, B.R.B. performed clinical studies. W.J.M. supervised the study. L.T.K., W.J.M. prepared the manuscript. L.T.K, C.T.L., C-C.S.P., R.S-C., S.H., J.I.L., C.D., Z.W., E.M., R.J.C., A.M.M., M.D., D.L.L., M.A., B.R.B., W.J.M. critically reviewed the manuscript.

DATA AND MATERIALS AVAILABILITY: All data associated with this study are in the main paper or supplementary materials. The datasets generated or analyzed in the current study are available in NCBI BioProject with accession ID PRJNA602524 and the European Nucleotide Archive with accession number PRJEB35495.

Overline: GVHD

[9]Division of Surgical Oncology, Department of Surgery, School of Medicine, University of California, Davis, CA, United States, 95817

[10]Department of Radiation Oncology, School of Medicine, University of California, Davis, CA, United States, 95817

[11]Tisch Cancer Institute, the Icahn School of Medicine at Mount Sinai, NY, United States, 10029

[12]Department of Medicine, Harvard Medical School, Boston, Massachusetts, MA, United States, 02115

[13]Department of Internal Medicine, School of Medicine, University of California, Davis, CA, United States, 95817

[14]Masonic Cancer Center; and Division of Blood and Marrow Transplantation, Department of Pediatrics; University of Minnesota, Minneapolis, MN, United States, 55455

Abstract

The efficacy of allogeneic hematopoietic stem cell transplantation (allo-HSCT) is limited by acute and chronic graft-versus-host disease (GVHD). The impact of obesity on allo-HSCT outcomes is poorly understood. Here, we report that obesity had a negative and selective impact on acute gut GVHD after allo-HSCT in mice with diet-induced obesity (DIO). These animals exhibited increased gut permeability, endotoxin translocation across the gut, and radiation-induced gastrointestinal damage after allo-HSCT. After allo-HSCT, both male and female DIO mouse recipients showed increased pro-inflammatory cytokine production and expression of the GVHD marker ST2 (IL-33R) and MHC class II molecules; they also exhibited decreased survival associated with acute severe gut GVHD. This rapid onset, obesity-associated gut GVHD depended on donor $CD4^+$ T cells and occurred even with a minor MHC mismatch between donor and recipient animals. Retrospective analysis of clinical cohorts who received allo-HSCT transplants from unrelated donors revealed that recipients with a high body mass index (BMI > 30) had reduced survival and higher serum ST2 concentrations compared to non-obese transplant recipients. Assessment of both DIO mice and allo-HSCT recipients with a high BMI revealed reduced gut microbiota diversity and decreased *Clostridiaceae* abundance. Prophylactic antibiotic treatment protected DIO mouse recipients from endotoxin translocation across the gut and increased inflammatory cytokine production, as well as gut pathology and mortality but did not protect against later development of chronic skin GVHD. These results suggest that obesity-induced alterations of the gut microbiota may impact GVHD after allo-HSCT in DIO mice, which could be ameliorated by prophylactic antibiotic treatment.

One-sentence summary:

Obesity and an altered gut microbiota are associated with worsened acute graft-versus-host disease outcomes in mice and humans.

Editor’s Summary:

Influencing stem cell transplant outcomes

Khuat et al. demonstrate that obesity worsens acute graft-versus-host disease (GVHD) outcomes in both mice and humans following allogeneic hematopoietic stem cell transplantation (allo-HSCT). Using a diet-induced obese (DIO) mouse model, the authors observed increased lethal GVHD targeting the gut. DIO mice had increased gut permeability, endotoxin translocation into the bloodstream and pro-inflammatory cytokine production, which correlated with reduced gut microbiota diversity. Manipulating the gut microbiota by antibiotic treatment partially protected DIO mice from lethal GVHD after allo-HSCT. Clinically, the authors found that patients with a high body mass index showed decreased gut microbiota diversity and poorer overall survival after allo-HSCT.

INTRODUCTION

Allogeneic hematopoietic stem cell transplantation (allo-HSCT) remains a widely used curative option for treating various hematologic diseases ranging from aplastic anemia to cancer. However, the high incidence of acute and chronic graft-versus-host disease (GVHD) remain major barriers associated with this approach (1). Acute GVHD (aGVHD) is caused by an inflammation-driven and often rapid multi-organ attack by donor T cells, whereas chronic GVHD (cGVHD) has a delayed onset and is dominated by fibrosis. The pathophysiologies of acute and chronic GVHD are distinct, but the mechanisms are not exclusive of one another. Central to both are immune-driven processes initiated by donor T cells in the recipient. Obesity has reached pandemic proportions with more than one-third of U.S. adults classified as obese with a body mass index (BMI) of 30 or higher (2). The impact of obesity on HSCT outcomes, either allogeneic or autologous, has been conflicting in part due to the numerous and constantly changing variables impacting HSCT regimens and the increasing age of recipients, particularly when HSCT is used for the treatment of malignancies. Limited sample size also contributes to lack of a clear effect of obesity on HSCT outcomes. One clinical study showed that the mortality rate after autologous HSCT (auto-HSCT) was lower in overweight and obese patients compared to the mortality rate in normal weight patients (3). Another study showed that pre-transplantation BMI was associated with a significantly greater risk of grade II-IV aGVHD in patients undergoing allo-HSCT (4). However, obesity has also been reported to be associated with higher survival rates after allo-HSCT (5), making definitive conclusions difficult. The increasing incidence of obesity among patients requiring HSCT, given recent reports that obesity in certain instances can result in increased survival following cancer treatments or immunotherapy has necessitated careful dissection of its impact (6, 7). This is particularly the case with preclinical assessment, because studies have only assessed obesity in the context of immune reconstitution and hematopoietic recovery following syngeneic HSCT (8, 9). Therefore, preclinical evaluation of obesity using different murine models, combined with correlation using clinical data in allo-HSCT, would enable mechanistic understanding of the impact of obesity and assessment of possible therapeutic interventions.

Obesity results in sterile, chronic inflammation, termed “meta-inflammation”, which has multiple effects both on immune cells and parenchymal tissues (10). In addition to obvious metabolic and hormonal effects, which can be exacerbated over time, there are strong immunomodulatory effects associated with obesity in which pro-inflammatory innate

pathways are augmented concurrently with suppressed adaptive immune responses. Previous studies with a diet-induced obese (DIO) mouse model reported that strong systemic immune stimulation, applied even in the absence of transplantation, resulted in a large macrophage-driven increase in cytokine production culminating in multi-organ pathology and death (11–13). However, in contrast, other reports examining obesity's impact during cancer immunotherapy involving immune checkpoint blockade surprisingly described increased anti-tumor effects and overall survival in cancer patients (6, 7). In one study, the improved outcome for obesity was observed in both mouse preclinical models and human clinical trials (7), suggesting that, although obesity may be deleterious to human health in the long term, certain situations may be exist for which the meta-inflammatory state and increased nutrient stores are beneficial. We therefore examined the impact of obesity following allo-HSCT on GVHD pathogenesis.

In this study, we set out to examine the impact of obesity following allo-HSCT on GVHD pathogenesis in mice and humans. We observed that DIO mice had increased gut permeability and endotoxin translocation across the gut as well as reduced gut microbiota diversity. Following allo-HSCT in the DIO mice, these changes resulted in accelerated aGVHD manifested by gastrointestinal (GI) tract pathology. DIO mice experienced severe aGVHD in an aGVHD model where donor and recipient mice had a major mismatch of major histocompatibility complex (MHC) antigens, and also in a cGVHD sclerodermatous model where donor and recipient mice had a minor histocompatibility antigen mismatch that normally does not result in aGVHD. In both mouse models, pathological assessment revealed substantial GI tract pathology in DIO mice correlating with lethality. The gut pathology depended on $CD4^+$ T cells, because lethal aGVHD was not induced in recipients receiving $CD8^+$ T cells alone or in $CD8^+$ T cell-dependent GVHD models. Analysis of a clinical cohort of patients undergoing allo-HSCT showed better overall survival (OS) in patients with a BMI less than 30. Our results suggest that obesity has an adverse effect on outcomes in mice and humans after allo-HSCT.

RESULTS

Obesity exacerbates GI aGVHD in a MHC-mismatched GVHD mouse model

Control or DIO C57BL/6 mice were fed a 10%-fat diet or 60%-fat diet, respectively for 4 to 6 months. DIO mice were heavier (fig. S1A), and the distribution of body fat differed between the two cohorts (Fig. 1A). Although DIO mice did not exhibit major metabolic dysfunction, they had significantly increased serum glucose concentrations compared to control mice (fig. S1B, $p<0.0001$). To initially assess the impact of obesity on GVHD, we used a total MHC-mismatch strain combination in which lethal aGVHD occurs affecting gut, liver, and skin (14). The mouse model involves transplantation of donor BALB/c ($H\text{-}2^d$) bone marrow cells and purified T cells into lethally-irradiated control or DIO C57BL/6 recipients ($H\text{-}2^b$) and we refer to this model as "BALB/c → C57BL/6 + T" (Table 1). The DIO recipients uniformly and rapidly succumbed to aGVHD within the first week after allo-HSCT; whereas the control mice developed aGVHD more slowly and some survived for more than 30 days (Fig. 1B–C and fig. S1C). Gross morphology indicated severe GI tract damage, and histological assessment showed markedly augmented aGVHD

pathology, specifically in the GI tract and not in the liver (Fig. 1D–G and fig. S1D). Serum cytokine measurements and quantification of gene expression demonstrated increased pro-inflammatory cytokines (IL-6 and TNF), as well as increased serum concentrations of the GVHD marker ST2, a marker of GI tract GVHD (15, 16), in the DIO recipients following allo-HSCT (Fig. 1H–J). There was marked expansion of donor $CD4^+$ T cells, but not $CD8^+$ T cells, in the mesenteric lymph nodes of the DIO recipients compared to the controls (Fig. 1K and fig. S1E). These data indicated that, in a model of aGVHD, obesity augmented lethal gut aGVHD pathogenesis, which was accompanied by $CD4^+$ T cell expansion and overproduction of pro-inflammatory cytokines.

Obesity induces GI aGVHD even in mouse strain combinations where only delayed chronic skin GVHD normally occurs

Aside from differences in kinetics, aGVHD and cGVHD are delineated by different pathophysiological pathways with aGVHD characterized by inflammatory pathology and cGVHD by fibrotic pathology (1). The MHC-matched but minor histocompatibility antigen mismatch strain combination of B10.D2 ($H\text{-}2^d$) donor cells into lethally-irradiated BALB/c recipients ($H\text{-}2^d$) has been well-described for the delayed development of sclerodermatous fibrotic cGVHD in the skin that does not affect other organs (17, 18). We assessed GVHD outcomes of control and DIO BALB/c recipients (fig. S2A–B). Whereas control recipients developed the typical delayed sclerodermatous skin GVHD (Fig. 2A–C), BALB/c DIO recipients succumbed to a rapidly lethal gut GVHD (Fig. 2D), resembling the rapidity and severity observed in the DIO recipients in the BALB/c → C57BL/6 + T model (Fig. 1, Table 1). Clinical symptoms of the BALB/c DIO mice were consistent with aGVHD and included diarrhea, body weight loss, ruffled fur, and severe hunching (Fig. 2E and fig. S2C). This rapid appearance of lethal, acute gut GVHD occurred in both male and female DIO recipients; both sexes rapidly succumbed (Fig. 2F and fig. S2D). In contrast, control recipients of either sex had a nonlethal sclerodermatous skin cGVHD that appeared 20 days after allo-HSCT (fig. S2E). Similar to the DIO recipients in the BALB/c → C57BL/6 + T model (Fig. 1D, E), the GI tract of the BALB/c DIO mice had an markedly abnormal histological structure in the small intestine and colon with the destruction of the epithelial mucus layer and GI crypts (Fig. 2G,H). This aGVHD lethality resulted from damage to the GI tract, and there was no evidence of liver pathology (Fig. 2I, J and fig. S2F). Increased pro-inflammatory cytokines (IL-6 and TNF) were also observed, as well as increases in ST2 (Fig. 2K–M), consistent with previously published data (15, 16).

We assessed if the increased lethality following allo-HSCT in the DIO mice was related to the high-fat diet rather than an increase in body weight. We compared outcomes of mice fed a high-fat or low-fat diet for 1 month or 4 months. Short-term consumption of the high-fat diet increased body weight (fig. S2G) but did not result in obesity and lethal aGVHD as was seen in the DIO mice fed a high-fat diet long-term (fig. S2G–I). Instead, the post allo-HSCT survival and inflammatory cytokine profiles of the mice fed a short-term high-fat diet were similar to those of mice fed a low-fat diet.

Consistent with the dependency of this aGVHD model on $CD4^+$ T cells (19), the BALB/c DIO recipients had increased numbers of donor $CD4^+$ T cells and not $CD8^+$ T cells (Fig. 2N

and fig. S2J). Correlating with the increased pro-inflammatory cytokines in the serum and ST2 in the GI tract, the donor T cells in the DIO mice had more proliferation capability (fig. S3A–B). Within the $CD4^+$ T cells in the mesenteric lymph nodes, most were T helper type 1 (T_H1), detected as T-bet^+ cells, and T helper 17 (T_H17), detected as RORγt^+ cells (fig. S3C–D).

Taken together, the results from the BALB/c→C57BL/6 + T mouse model and the B10.D2→BALB/c + SC mouse model demonstrated that obesity altered the GVHD paradigm, regardless of recipient strain. Furthermore, obesity shifted GVHD pathogenesis from the typical skin cGVHD into a lethal rapid GI tract aGVHD associated with $CD4^+$ T cell expansion and increased production of cytokines.

Obesity correlates with worse GVHD outcomes in adult patients after allo-HSCT

To build on the preclinical data demonstrating higher GVHD induction with obesity, GVHD outcomes in adult patients who underwent unrelated allogeneic HSCT at the University of Minnesota were stratified based on their BMI before allo-HSCT (Fig. 3A and table S1). The results showed that transplant-related mortality (TRM) at 1 year was ~ 5 times higher in patients with BMI >30 (26%) versus those with BMI < 30 (5%) (Fig. 3B). We also evaluated the patient cohort using the serum ST2 marker at baseline, that is, before conditioning chemotherapy or radiation prior to transplant, and BMI. We separated the cohort into two groups: One group had BMI > 30 and high baseline ST2, which we established as > 35 pg/ml using recursive partitioning to set the threshold, the other group had a baseline ST2 below this threshold. Baseline ST2 alone was not associated with survival (fig. S4), but patients who were both obese (BMI>30) and had a high baseline ST2 had markedly worse survival: 36% at 1 year versus 81% survival for all others (Fig. 3C). Histological assessment also revealed significantly worse GVHD severity in patients with BMI > 30 (Fig. 3D). Analysis of GVHD serum marker ST2 (15) with an unrelated allo-HSCT patient cohort (Tisch Cancer Institute at Mount Sinai) at day 7 post allo-HSCT also showed increased ST2 concentrations in obese patients (BMI >30) compared to those with BMI less than 30 (table S1 and Fig. 3E–F). These results indicated that the clinical outcome data mirrored our preclinical findings showing that obesity correlated with poorer outcomes after allo-HSCT.

Donor $CD4^+$ T cells mediate gut aGVHD in obese mouse recipients

GVHD induction using either the B10.D2-->BALB/c or BALB/c-->C57BL/6 strain models (Table 1) depends on donor CD4+ T cells (14, 17, 20). To verify that $CD4^+$ T cells were responsible for increased aGVHD pathology in the DIO recipients, allo-HSCT was performed comparing transfer of bone marrow with whole splenocytes, or purified $CD8^+$ T cells only, or purified $CD4^+$ T cells only in the B10.D2→BALB/c model (Table 1). $CD8^+$ T cell transfer did not result in any aGVHD in the DIO recipients (Fig. 4A–C). In contrast, transplant with either whole splenocytes (Fig. 4A–C) or $CD4^+$ T cells (fig. S3E–F) resulted in lethal aGVHD but only in the DIO mice. To confirm the requirement for $CD4^+$ T cell responses in gut aGVHD in the DIO recipients, we used another minor mismatch strain combination consisting of C3H.SW-->C57BL/6 (Table 1), which results in aGVHD affecting liver and skin mediated solely by $CD8^+$ T cells (18, 20–22). The DIO and control recipients were transplanted with either total T cells ($CD4^+$ and $CD8^+$) or $CD8^+$ T cells

alone (18). Using the C3H.SW->C57BL/6 model, the transfer of donor $CD8^+$ T cells or total T cells into either DIO or control recipients resulted in comparable skin aGVHD (Fig. 4C–E and fig. S5A). In contrast to when MHC allogeneic donors (BALB/c) were used in these recipients (Fig. 1), there was no evidence of gut pathology or increased cytokine production in the DIO recipients of either $CD8^+$ T cells or total T cells (Fig. 4F–H and fig. S5A–B). Histological assessment revealed comparable liver GVHD pathology both in control and DIO mice (fig. S5A, C, D, E). These results indicate that obesity may have predisposed the recipient mice to gut aGVHD mediated by donor $CD4^+$ T cells.

Obesity increases gut permeability and epithelial cell apoptosis after cytoreductive conditioning

Either a “Western diet” (high fat, high sugar) or a high-fat diet alone predisposes mice to increased intestinal permeability (23–25). Given the specific targeting of the GI tract by aGVHD in the obese recipients, we examined the impact of a high-fat diet on aGVHD induction and the role of the cytoreductive conditioning regimen (total body irradiation, TBI). DIO mice displayed increased intestinal permeability and translocation of lipopolysaccharide (LPS) indicated by higher LPS-binding protein (LBP) and endotoxin concentrations in the serum of DIO versus control mice on day 2 after irradiation (Fig. 5A, B). There were also increases in apoptotic cells in the intestines of DIO mice within 48 hours of irradiation (Fig. 5C–F). There was also evidence of increased activation of the innate immune system with marked dendritic cell (DC) activation, indicated by increased MHC staining, in the DIO BALB/c mouse recipients following allo-HSCT (Fig. 5G–H and fig. S6A–B). Compared to $CD4^+$ T cell transplantation in control mice, transplantation with $CD8^+$ T cells in control mice resulted in a decreased number of activated DCs in the mesenteric lymph nodes (fig. S6C–D). These data suggest that obesity predisposed mice to increased intestinal permeability and cellular apoptosis following cytoreductive conditioning by irradiation, which resulted in increased activation of antigen-presenting DCs in the intestine after allo-HSCT.

Obesity correlates with a less diverse gut microbiota and GVHD-associated bacterial taxa in mice

The gut microbiota impacts not only cancer immunotherapy but also GVHD and HSCT outcomes (26, 27). High-fat diet consumption and obesity alter the gut microbiota (24, 28); therefore, we assessed the gut microbiota profiles in mice fed a short-term low-fat versus high-fat diet, as well as the gut microbiota profiles of DIO mice versus control mice in two mouse strains. The gut microbiota profiles of DIO BALB/c and DIO C57BL/6 mice before allo-HSCT were remarkably similar in terms of multiple taxonomic units (Fig. 6A). All DIO mice exhibited a distinct and less diverse gut microbiota profile compared to the control mice (Fig. 6B–C). Short-term consumption of a high-fat diet by BALB/c mice also resulted in a distinguishable change in gut microbiota profile (fig. S7A–B) and reduced gut microbiota diversity compared to mice fed a low-fat diet for the same period of time (fig. S7C–D).

The abundance of the family *Clostridiaceae* correlates with improved GVHD outcomes (27). We found this family of bacteria was reduced in both DIO BALB/c and DIO C57BL/6

mice compared to the controls (Fig. 6D–E, fig. S8A) and in mice fed a short-term high-fat diet compared to mice fed a low-fat diet (fig. S7E). In contrast, the relative abundances of GVHD-associated *Akkermansia muciniphila* (26, 29) were increased in BALB/c mice fed a short-term high-fat diet compared to mice fed a low-fat diet (fig. S7F), and in DIO BALB/c mice compared to the control BALB/c mice (Fig. 6A, fig. S8A). The relative abundance of *Enterococcus*, the genus that is mainly found post allo-HSCT and correlates with poor GVHD outcomes (30), significantly increased in the fecal samples from DIO mice post allo-HSCT compared to the controls (Fig. 6F, p=0.0096).

In a different patient cohort from the University of Minnesota (table S2), we evaluated the pre-HSCT gut microbiota profile of patients stratified by BMI. Although we did not observe a significant difference in gut microbiota profiles or diversity using a BMI of 30 as the cut-off (fig. S8B–C), we found significant microbiota alterations in obese patients with BMI > 30 compared to lean patients with a BMI < 25 (Fig. 6G, $p < 0.05$). Gut microbiota sequencing analysis pre-HSCT demonstrated a significant decrease of microbial diversity and a distinct profile in obese patients compared to lean patients (Figure 6G and fig. S8D–E), and also a significantly lower abundance of genus *Clostridium* in obese patients (Fig. 6H), consistent with a well-described risk factor for worse GVHD outcomes post-HSCT (31, 32). These consistent gut microbiota patterns between obese mice and humans suggested that gut microbiota profiles as well as body fat composition may be contributing factors to the increase in gut aGVHD observed in DIO mouse recipients after allo-HSCT.

Prophylactic antibiotic treatment before transplant ameliorates aGVHD but not cGVHD in DIO mouse recipients

Given these gut microbiota differences between control and DIO mice, as well as the increased endotoxin translocation from the gut into the bloodstream in the DIO mice after total body irradiation, we hypothesized that prophylactic antibiotic administration could be protective provided enough time was given for restoration of intestinal permeability before allo-HSCT. Using the B10.D2→BALB/c + SC model, DIO and control mice were given a regimen of antibiotics (ampicillin, vancomycin, and neomycin) two weeks before HSCT, which is comparable to several months treatment in humans. Prophylactic antibiotic administration did not affect donor cell engraftment (fig. S9) and markedly ameliorated GVHD lethality; ~50% of DIO mice were protected from the rapid lethality that occurred in untreated DIO mice (Fig. 7A–B).

Gut microbiota assessment revealed distinct gut microbiota profiles in control mice, DIO mice, and DIO mice treated with antibiotics without irradiation and transplantation for both BALB/c and C57BL/6 mouse strains (Fig. 7C and fig. S10A–B). Whereas the gut microbiota of DIO mice displayed dominance of the GVHD-associated *Akkermansia muciniphila* (29) species, antibiotic treatment reduced the relative proportion of this strain in the gut microbiota before and after allo-HSCT (Fig. 7D). Bacterial load was significantly reduced in DIO mice after antibiotic administration (Fig. 7E). Furthermore, antibiotic treatment reduced the amounts of pro-inflammatory cytokines, ST2, and endotoxin in recipient DIO mice (Fig. 7F–H). Compared to untreated recipient DIO mice, antibiotic-treated, recipient DIO mice also showed decreased DC activation (MHC^+ cells) and overall

numbers of DCs in the mesenteric lymph nodes, but not in the spleen (fig. S11A–D). Similar to the control recipient mice, the antibiotic-treated DIO recipients that survived allo-HSCT subsequently developed sclerodermatous skin cGVHD (Fig. 7B and fig. S11E–F).

Adipocytes of BALB/c mice are radiosensitive (33), and following HSCT there was consistent weight loss in the DIO BALB/c recipients both with and without antibiotic pre-treatment and even when the mice were fed the high-fat diet. Consequently, there were no weight differences between the groups at the later time-points when the chronic skin GVHD occurred (fig. S11G).

These data indicated that gut microbiota alterations were observed in both obese mice and humans. In mice, the combination of a high-fat diet and higher body fat deposition resulted in gut microbiota alterations that played a dominant role in the induction of gut aGVHD and poorer outcomes, which were partially ameliorated with antibiotic prophylaxis.

DISCUSSION

HSCT is currently used for the treatment of various disorders, particularly hematologic malignancies. Allo-HSCT represents one of the first examples of successful cellular immunotherapy. However, both aGVHD and cGVHD, which have different pathophysiological pathways, still represent major clinical hurdles. Advances in HLA typing, modifying conditioning regimens, and post-HSCT support have markedly improved outcomes, yet basic questions on the potential impact of age and BMI on HSCT still remain unclear. Patient demographics and profiles are rapidly changing with obesity reaching pandemic proportions. The impact of obesity both on overall health and immune status are complex and multifactorial. Obesity is associated with a meta-inflammatory state associated with general immunosuppression and is considered a poor prognostic indicator for many human health conditions. We and others have shown in preclinical models that obesity results in exacerbated inflammatory responses following systemic immunostimulation or sepsis culminating in a lethal production of cytokines and death from multi-organ pathology (11–13). However, the complexity of the effects of obesity on immune responses is highlighted by reports showing a potentially positive impact in cancer following immune checkpoint blockade due to increased anti-tumor effects and overall survival (6, 7). Thus, it is critical to assess the impact of obesity using different immune-mediated scenarios or processes.

The results presented here, using both mouse preclinical models and clinical outcomes, indicated that obesity has a “net” negative effect on allo-HSCT outcomes in both mice and humans. We found that obesity was associated specifically with increased aGVHD affecting the GI tract. This effect appeared restricted to the gut and relied on donor $CD4^+$ T cells and was associated with increased production of proinflammatory cytokines. Thus, in contrast to the systemic immune stimulation models and sepsis in which obesity is associated with multi-organ tissue damage (lung, liver, and gut) (11), in allo-HSCT the effects of obesity were limited to the GI tract. We propose that this GI-selective effect of obesity is likely due to the use of cytoreductive conditioning that directly caused gut tissue damage as well as endotoxin translocation across the gut epithelia. We were surprised to find that this

rapid severe gut aGVHD pathology and lethality occurred in a preclinical mouse strain combination more commonly used to assess later skin cGVHD (17, 18). The relatively modest experimental alteration of adding obesity as a condition of the mouse recipient resulted in a greatly altered outcome such that the obesity-including model resembled a major MHC-mismatched strain combination. There appeared to be a critical narrow window in which the gut aGVHD led to lethality in DIO mice, because the survivors of aGVHD later developed skin cGVHD, albeit to a lesser extent compared to control recipients. This effect of obesity was specific for the gut because even in strain combinations that developed aGVHD in liver and skin, the DIO recipients did not exhibit exacerbated pathology. Obesity has a multifactorial impact on the GI system influencing gut motility, hormone release, gut permeability, and radiation sensitivity (23, 24). Our data indicated that obesity-associated gut microbiota alterations rendered the GI tract more vulnerable to aGVHD after allo-HSCT. Our study also addressed the effect of obesity on cGVHD. Our results indicated that obesity had a negligible effect on cGVHD, because DIO mice that were protected from gut aGVHD through prophylactic antibiotic treatment still manifested the fibrotic skin cGVHD. This was not surprising given the distinct pathologic processes between acute (inflammatory) and chronic (fibrotic) GVHD, as well as the immune cells involved.

The gut microbiota has been under investigation for immune effects, both positive and negative. In the setting of HSCT, several studies using different types of antibiotics and treatment strategies have resulted in different GVHD outcomes in mice and in patients (26, 29, 34–36). Our results indicated that the restricted gut microbial diversity associated with obesity in both mice and humans had a negative impact on allo-HSCT outcomes. In that regard, the gut microbiota’s effects in DIO mice from different strains were remarkably similar. Indeed, both DIO mice and obese humans shared common features. Various regimens have been tested to define the optimal gut microbiota composition to lessen GVHD (26, 27). We did not observe any benefit from antibiotics for GVHD in lean mice; only in the DIO recipients was partial protection observed. Thus, BMI should be considered when testing antibiotic and gut microbiota-targeted regimens.

Intestinal microbiota changes are not only associated with obesity but also with aging (37). Therefore, it is important to delineate the parameters of aging and obesity on allo-HSCT and incorporate human-modifying factors into the mouse models because the combination of both aging and obesity may amplify the pro-inflammatory responses and pathology. The similar gut microbiota alterations, increases in markers such as ST2, and similar HSCT outcomes observed in both DIO mice and patients with a high BMI supported the potential relevance of mouse preclinical HSCT models. However, many variables arise in clinical HSCT that are not reflected in these mouse models.

There are several limitations to our study. One limitation relates to the patient clinical data used here as all but one case involved unrelated allo-HSCT, which is associated with much poorer outcomes (38). Thus, future studies will need to assess if obesity correlates with ST2 and outcomes in more commonly used and less severe allo-HSCT modalities, such as with related donors. In such cases, obesity may impact overall efficacy, which could include cancer progression and relapse. We also did not include co-morbidities that are often associated with obesity and that could contribute to poorer outcome. We did not

assess factors associated with low BMI that may contribute to better outcomes. Additionally, several questions remain unanswered. We did not investigate the impact of body fat content and metabolism on donor T cell activation and GVHD outcomes. A high-fat diet increases fatty acid oxidation in DIO mice (39) and fatty acid metabolism is important for T cell function in GVHD (40). Therefore, it raises the question of whether the obese environment provides resources that enhance donor T cell activation and potentially that of myeloid cells that contributes to GVHD pathology. Another limitation is that we did not investigate the mechanism by which body fat deposits versus the high-fat diet itself influenced rapid aGVHD. We found that non-obese mice that consumed a high-fat diet for one-month did not succumb to the rapid aGVHD in the minor-MHC mismatch model; whereas their obese counterparts did. Despite performing tests with multiple mouse strains with different durations of a high-fat diet and obese and lean conditions, there are many more variables to test. These include the duration of the high-fat diet with development of more pronounced metabolic alterations, the impact of age, the composition of the diet (high fat only versus a Western diet with high sugar as well), mouse strain susceptibility differences to the cytoreductive conditioning (and type) and the different strain combinations of our preclinical models.

The results presented here showed that obesity has a multifactorial impact on allo-HSCT, with an overall negative effect due to gut aGVHD. This GI-targeted aGVHD depended on $CD4^+$ T cells and resulted in decreased survival in both mice and humans. In mice, therapeutic intervention using a prophylactic antibiotic regimen partially prevented or ameliorated lethal GI aGVHD. Our study indicated that obesity and the associated gut microbiota alterations affected immunopathology resulting from exacerbated pro-inflammatory responses. Thus, the gut microbiota-associated alterations may represent a potential target for therapeutic intervention in GVHD subsequent to allo-HSCT.

MATERIALS AND METHODS

Study design

7 to 8-week-old BALB/c ($H\text{-}2^d$) and C57BL/6 ($H\text{-}2^b$) male and female mice were used in this study. For each experiment, at least two experimental replicates were performed. Mice were selected and assigned to their groups based on their body weights at the time each experiment started. Treatment with antibiotics was assigned from the beginning of each experiment after selecting DIO mice (half of DIO mice received antibiotics in drinking water, the other half consumed normal water). Histology samples were evaluated and scored by a pathologist in a blinded manner. All studies using mice were approved by UC Davis Institutional Animal Care and Use Committee (IACUC).

The study of GVHD outcomes post allo-HSCT and correlation between pre-transplant ST2 levels and survival in patients stratified by BMI was analyzed retrospectively with data obtained from 37 patients (22 BMI<30, 15 BMI>30) at University of Minnesota (Table S1). Comparison of ST2 levels between 5 BMI<30 and 5 BMI>30 patients post unrelated allo-HSCT was performed at The Tisch Cancer Institute – Mount Sinai (Table S1). The study of obesity and microbiota diversity pre-transplant was conducted at University of

Minnesota from 18 patients (4 BMI<30, 14 BMI>30, Table S2). All studies were approved by the University of Minnesota and Mount Sinai Institutional Review Boards.

Patient cohorts

The effect of serum ST2 and obesity on post-transplant survival was assessed in 37 adult patients undergoing unrelated donor allo-HSCT, who subsequently developed aGVHD. Assessment of pre-transplant fecal microbiota diversity and its relationship with obesity was determined in an independent cohort of patients participating in a prospective stool sample collection study. For aGVHD histological assessment, formalin-fixed, paraffin-embedded intestinal tissues of patients with biopsy-proven aGVHD from the University of Minnesota were analyzed for histological severity according to Lerner criteria (41). Clinical details of the histological cohort have been published (42). Pre-transplant fecal samples from patients undergoing HSCT were collected prospectively during the course of the University of Minnesota Institutional Review Board-approved study MT2015–08R (Table S2). In another clinical study at Tisch Cancer Institute, the Icahn School of Medicine at Mount Sinai (15), patients from the Mount Sinai Acute GVHD International Consortium (MAGIC) underwent allo-HSCT and provided blood samples for a biorepository 7 days after transplant. We stratified 10 patients undergoing unrelated and related mismatched allo-HSCT based on their BMI (BMI < 30 and BMI > 30) and compared their GVHD-associated marker ST2 in their serum at day 7 after allo-HSCT. Serum samples from Mount Sinai patients were obtained as part of a natural history study of allo-HSCT recipients designed to correlate serum GVHD biomarkers with clinical outcomes. Briefly, clinical data including pre-transplant patient characteristics, weekly GVHD staging and immunosuppression medications, were collected weekly until day 100 post allo-HSCT. Serum samples were collected weekly until day 28 post allo-HSCT, and then on day 56 and day 90 post allo-HSCT. Serum samples were aliquoted into 0.5 ml vials and stored at −80C until analyzed.

Mice and allo-HSCT

7- to 8-week-old BALB/c (H-2^d) and C57BL/6 (H-2^b) male and female mice used in this study were obtained from Taconic Biosciences (Germantown, NY, USA). All mice were maintained at the University of California, Davis Medical Center's vivarium in accordance with Institutional Animal Care and Use Committee (IACUC) standards.

Mice were placed on a high-fat (60% fat from lard) diet or low-fat (10% fat) diet (D12492 or D12450J, Research Diets, Inc., respectively) for 4 – 6 months to create DIO and control mice. Mice, 8 to 12 weeks old, in the strains B10.D2 (H-2^d), BALB/c (H-2^d), and C3H.SW (H-2^b) were obtained from Jackson Laboratory (Bar Harbor, ME, USA) and used as donor mice. To create minor MHC-mismatched GVHD models, BALB/c mice ($H2^d$) received lethal total body irradiation (TBI, 800 cGy; ^{137}Cs source) and underwent transplantation with bone marrow cells with or without splenocytes ($10 – 25 \times 10^6$), or purified $CD4^+$ T cells (2×10^6), or purified $CD8^+$ T cells (2×10^6) from donor B10.D2 mice ($H2^d$); C57BL/6 mice ($H2^b$) received lethal TBI (1050 cGy; X-ray source) and T cell-depleted bone marrow cells with or without purified $CD8^+$ T cells (3×10^6) or purified T cells (3×10^6) from C3H.SW mice ($H2^b$). To create major MHC-mismatched GVHD model, C57BL/6 mice ($H2^b$) received lethal TBI (1050 cGy; X-ray source) and T cell-depleted bone

marrow cells with or without purified T cells ($4.5–9 \times 10^6$) from donor BALB/c mice ($H2^d$). Ampicillin (Cat# A5354), Neomycin (Cat# N5285), and Vancomycin (Cat# V2002) were from Sigma, St. Louis, MO, USA, and the antibiotics were added to drinking water at the final concentration of 0.5 mg/ml for 14 days before allo-HSCT.

MRI data acquisition and image analysis

Mice were anesthetized with isofluorane and oxygen then scanned on a Biospec 70/30 7.0 Tesla small-animal MRI system (Bruker Biospin Inc) using a 60-mm quadrature transmitter/receiver coil for whole-body imaging. The scanning protocol consisted of the multi-slice with multi-echo (MSME) spin-echo sequence with a single echo and with respiratory gating to minimize breathing artifacts. Scan parameters were TE 7.062, TR 775, conducted with and without chemical-selective fat suppression. Slice images were obtained in the coronal direction to improve spatial resolution while keeping scan time and TR at minimums. The in-plane matrix was 200×267 with a resolution of 0.3×0.3 mm. Forty-four slices were acquired with a slice thickness of 0.6 mm. Field of view was $6 \times 8 \times 2.64$ cm. Difference images were generated by subtracting the fat-suppressed images from the non-fat-suppressed images to identify the 3D distribution of fat deposits. Physiological monitoring (temperature and respiration) was used during the entire scan to ensure consistency and animal physiological stability.

aGVHD and cGVHD clinical scoring criteria

aGVHD clinical scores were determined based on weight loss (0 – 2), hunching (0 – 2), diarrhea (0 – 2), fur texture (0 – 2), and skin integrity (0 – 2) (43). Individual mice were euthanized if they had a total score over 7 out of 10 or showed severe hunching.

For sclerodermatous cGVHD, BALB/c mice were monitored for skin clinical scores and body weight loss after allo-HSCT as described previously (44). Briefly, skin clinical score was assigned as follows: 0, healthy appearance; 1, skin lesions with alopecia area < 1 cm^2; 2, skin lesions with alopecia area of 1 to 2 cm^2; 3, skin lesions with alopecia area > 2 cm^2. Tail, ear, or paw scaling represented an additional 0.3 point for each lesion. Mice with a clinical skin score > 3.3 (on a scale of 0 to 3.9) or with severe ischemic skin and tail lesions and hunching were euthanized per guidelines.

Histology and histopathology scores

Tissues harvested from the mice were placed in 10% formalin, embedded in paraffin, sectioned, and stained with hematoxylin and eosin. Tissue sections were evaluated and graded by a board-certified pathologist in a single-blinded fashion. Skin pathology was scored on a scale of 0 to 10, based on dermal fibrosis (0 to 2), fat atrophy (0 to 2), inflammation (0 to 2), epidermal interface change (0 to 2), and follicular dropout (0 to 2). GI pathology was scored on a scale of 0 to 4, based on the crypt epithelium apoptosis, lymphocyte infiltration, extent of fibrosis and inflammation, and mucosal necrosis. Fibrotic skin samples were assessed by Masson’s Trichrome staining with Masson’s 2000 Trichrome kit (SKU# KTMTR2, American MasterTech, Lodi, CA, USA). Images were visualized with a Vanox AHBS3 microscope with a SPlan Apo 20×/0.70 NA objective (Olympus, NY, USA)

and acquired with a SPOT RT color digital camera using SPOT version 4.0.2 software (Diagnostic Instruments, MI, USA).

Terminal deoxynucleotidyl transferase dUTP nick end labeling (TUNEL)

TUNEL assay was performed using ApopTag Plus Peroxidase In Situ Apoptosis Detection Kit (EMD Millipore, Cat No. S7101) for the detection of apoptotic cells. Briefly, the colon was harvested from non-irradiated and 48 hours after irradiation from lean and obese mice. The tissues were washed and fixed in 10% formalin and paraffin embedded. The manufacturers' protocol was followed for TUNEL staining. The chromogenic DAB substrate labeled the apoptotic bodies with permanent, intense brown color, which was detected using bright field microscope (Olympus, PA, USA). For each mouse, the images were acquired at three regions along the proximal colon, transverse colon, and distal colon. From each region, between 9 – 11 high power (20× fields) were used to count the bright, intense brown dots (apoptotic bodies). The count was normalized with the area from where the images were obtained, and data were represented as apoptotic bodies per mm^2.

Glucose measurement

Serum glucose was measured by Glucose HK Gen.3 kit (Cat# 04404483, Roche Diagnostics, Indianapolis, IN, USA) and analyzed by the COBAS INTEGRA 400 PLUS (Roche Diagnostics, Indianapolis, IN, USA).

Isolation of T cell subsets

T cells labelled with Thy1.2 antibody (clone 30-H12, eBiosciences, San Diego, CA) were depleted from the bone marrow using rabbit complement (CL 3442, Cedarlane Laboratories, Burlington, Canada). Mouse T cells, $CD8^+$ T cells, and $CD4^+$ T cells were isolated after negative selection using EasySep Mouse T cell isolation kit (Cat# 19851A), EasySep Mouse $CD8^+$ T cell isolation kit (Cat# 19853A), and EasySep Mouse CD4 T cell isolation kit (Cat# 19852). We used EasySep Magnet (Cat#18001) from StemCell Technologies (Vancouver, Canada) as the magnet for cell isolation.

Antibodies and flow cytometry analysis

Flow cytometry was performed as described previously. In brief, single-cell suspensions (1 million cells) were first incubated with Fc Block (BD Pharmingen, San Diego, CA, USA) for 10 minutes, then co-incubated with antibodies for 20 minutes at 4°C, followed by washing with staining buffer (PBS + 1% fetal bovine serum). Flow cytometry analysis was performed with the LSRFortessa cell analyzer (BD Biosciences, San Jose, CA, USA), and data were analyzed using FlowJo v10 software (FlowJo, Ashland, OR, USA). We used the following fluorochrome-conjugated monoclonal antibodies purchased from Biolegend (San Diego, CA, USA): CD45-Pacific Blue (30-F11), CD3-BV785 (17A2), CD4-BV711 (RM4–5), CD8-BV605 (53–6.7), CD86-FITC (GL-1), CD11c-PE/Cy7 (N418), I-A/I-E-APC/Cy7 (M5/114.15.2), T-bet-APC (4B10). We used the following fluorochrome-conjugated monoclonal antibodies purchased from from BD Biosciences (San Jose, CA, USA): CD229.1-PE (30C7), RORγt-PE-CF594 (Q31–378). We used fluorochrome-

conjugated monoclonal antibodies purchased from Invitrogen (San Diego, CA, USA): Ki-67-eFlour™ 450 (SolA15).

For Annexin V and propidium (PI) staining, single-cell suspensions ($1 – 5 \times 10^6$ cells/ml were stained with Annexin V-Pacific Blue (Biolegend Cat# 640918, San Diego, CA, USA). Cells then were incubated in dark for 15 minutes and stained with PI (Life Technologies, Ref# P3556) following manufacturer's protocol and were analyzed by flow cytometry within 10 minutes.

Quantitative polymerase chain reaction (q-PCR)

RNA was extracted from the GI and liver tissue using Qiagen RNeasy Mini kit (Cat# 74104, Qiagen, Valencia, CA, USA) according to manufacturer specifications. RNA was quantified using Qubit 4 RNA Broad range (ThermoFisher Scientific, Grand Island, NY, USA) and converted to cDNA using High Capacity RNA-to-cDNA kit (Ref# 4387406, Applied Biosystems, Foster City, CA, USA) following standard protocols. qPCR was performed on a StepOnePlus Realtime PCR System Applied Biosystems, Foster City, CA, USA) with Power SYBR Green PCR Master Mix (Ref# 4367659, Applied Biosystems, Foster City, CA, USA). *Glyceraldehyde 3-phosphate dehydrogenase* (*GAPDH*) (PPM02946E, Qiagen, Valencia, CA, USA) was used as the housekeeping gene.

ELISA and cytometric bead array (CBA)

Serum cytokines were measured by CBA flex set kits (BD Biosciences, San Jose, CA, USA): mouse TNF (Cat# 558299) and mouse IL-6 (Cat# 558301). Serum samples were diluted 1:4 using the assay diluent solution provided in the kit. Capture beads and detection beads were added as described in the manufacturer's protocol. Cytokine concentration was measured by flow cytometry with the LSRFortessa cell analyzer (BD Biosciences, San Jose, CA, USA). Mouse LBP and ST2 in the serum were measured using ELISA kits from Biometec GmbH, Greifswald, Germany (Cat# 043) and Invitrogen (by ThermoFisher Scientific, San Diego, CA, USA, Cat# 88–9334-88), respectively. Human ST2 concentrations were measured as previously described (15).

Mouse gut microbiota analysis

DNA was isolated using the Qiagen DNeasy PowerSoil kit (Qiagen) with the following modifications. After addition of buffer C1, samples were incubated at 65°C for 10 minutes then subjected to homogenization using a Biospec Mini-Beadbeater (Biospec Products) for 2 minutes. An additional wash step with 100% ethanol was included preceding the wash with kit buffer C5. Samples were eluted in 100 μl of buffer C6. Primers 319F (**TCGTCGGCAGCGTCAGATGTGTATAAGAGACAG**(spacer)*GT*ACTCCTACGGGAGGCAGCAGT) and 806R (**GTCTCGTGGGCTCGGAGATGTGTATAAGAGACAG**(spacer)*CC*GGACTACNVGGGTWTCTAAT) were used to amplify the V3-V4 domain of the 16*S* rRNA using a two-step PCR procedure. In step one of the amplification procedure, both forward and reverse primers contained an Illumina tag sequence (bold), a variable length spacer (no spacer, C, TC, or ATC for 319F; no spacer, G, TG, ATG for 806R) to increase diversity and improve the quality of the sequencing run, a linker sequence (italicized), and the 16*S* target sequence

(underlined). Each 25 μl PCR reaction contained 1 Unit Kapa2G Robust Hot Start Polymerase (Kapa Biosystems), 1.5 mM $MgCl_2$, 0.2 mM final concentration dNTP mix, 0.2 μM final concentration of each primer, and 1 μl of DNA for each sample. PCR conditions were an initial incubation at 95°C for 3 min, followed by 25 cycles of 95°C for 45 s, 50°C for 30 s, 72°C for 30 s, and a final extension of 72°C for 3 min. In step two, each sample was barcoded with a unique forward and reverse barcode combination using forward primers (**AATGATACGGCGACCACCGAGATCTACAC**NNNNNNNNTCGTCGGCAGCGTC) with an Illumina P5 adapter sequence (bold), a unique 8 nt barcode (N), a partial matching sequence of the forward adapter used in step one (underlined), and reverse primers (**CAAGCAGAAGACGGCATACGAGAT**NNNNNNNNGTCTCGTGGGCTCGG) with an Illumina P7 adapter sequence (bold), unique 8 nt barcode (N), and a partial matching sequence of the reverse adapter used in step one (underlined). The PCR reaction in step two contained 1 Unit Kapa2G Robust Hot Start Polymerase (Kapa Biosystems), 1.5 mM $MgCl_2$, 0.2 mM final concentration dNTP mix, 0.2 μM final concentration of each uniquely barcoded primer and 1μl of the product from the PCR reaction in step one diluted at a 10:1 ratio in water. PCR conditions were an initial incubation at 95°C for 3 min, followed by 8 cycles of 95°C for 30 s, 58°C for 30 s, 72°C for 30 s, and a final extension of 72°C for 3 min. The final product was quantified on the Qubit instrument using the Qubit Broad Range DNA kit (Invitrogen) and individual amplicons were pooled in equal concentrations. The pooled library was cleaned utilizing Ampure XP beads (Beckman Coulter), then the band of interest was further subjected to isolation by gel electrophoresis on a 1.5% Blue Pippin HT gel (Sage Science). The library was quantified by qPCR followed by 300-bp paired-end sequencing using an Illumina MiSeq instrument (Illumina) in the Genome Center DNA Technologies Core, University of California, Davis. DNA extractions and library preparation were performed by the UC Davis Host Microbe Systems Biology Core Facility.

Heatmaps were generated with R package ‘pheatmap’. Boxplots and volcano plots were created with R. The linear discriminate effect size (LEfSe) program was used to identify differentially abundant taxa between the groups (45). The LEfSe program uses the Kruskal-Wallis sum-rank test to detect taxa with significant differential abundance in relation to class and then biological significance is determined by pairwise tests between subclasses using the Wilcoxon rank-sum test. Finally, linear discriminate analysis is used to estimate effect size of each differentially abundant taxa and taxonomic cladograms generated to highlight significant differences in taxa.

Human fecal microbiota analysis

Pre-transplant fecal samples from patients undergoing HSCT were collected prospectively during the course of the University of Minnesota Institutional Review Board-approved study. Patients were included in this analysis if they had a fecal sample collected at baseline (pre-conditioning). Of the 26 total patients who met these criteria, 11 were female and 15 were male. For the analyses, these patients were stratified into lean (BMI < 25; N = 4), overweight (BMI 25–30; N = 8), and obese (BMI > 30; N = 14). The median age of the recipients was 60 years (range 25 – 73 years). Fecal samples were submitted to the University of Minnesota Genomics Center (UMGC) for DNA extraction and sequencing, performed using the Illumina NeoPrep library system. Sequencing was performed on an Illumina HiSeq with

the 2×125 v4 kit. Raw forward reads were quality controlled and converted to FASTA using SHI7 v0.9.9 (46), with a quality filter threshold of 37 and length 80. Bacterial taxonomic assignments were identified by aligning all processed reads against a custom database of human-associated bacterial species and genera obtained from the comprehensive NCBI RefSeq database release 87 (47). Alignments were performed at 98% identity using the exhaustive, optimal alignment tool BURST (https://github.com/knights-lab/BURST). Rare operational taxonomic units (OTUs) (less than 1% prevalence) and low-depth samples (< 20,000 counts) were removed in R, and alpha diversity metrics were calculated on rarefied OTU tables using QIIME2 v2018.6.0. All other analyses were performed in R using the packages *vegan* and *ggplot2* after centered log ratio (CLR) transformation.

Statistics

Mouse weight loss, skin clinical scores, and quantitative tumor burdens were analyzed by two-way analysis of variance (ANOVA) with Tukey's post hoc test for comparison among groups. Nonparametric Mann-Whitney test was used to compare two unpaired groups. A p value of < 0.05 was considered significant. Kaplan-Meier survival curves were analyzed by a log-rank test. Data were graphed and statistically analyzed using GraphPad Prism V6.02 (GraphPad Software, Inc., CA, USA).

Supplementary Material

Refer to Web version on PubMed Central for supplementary material.

ACKNOWLEDGEMENTS

We would like to thank Drs. Leslie S. Kean, Alice F. Tarantal, Andreas J. Bäumler, Renée M. Tsolis, Michael Lawson, and Sean Judge for their expertise and insightful feedback and suggestions. We also would like to thank Weihong Ma and Logan Vick from the Murphy lab; Shuaib Juma from the UC Davis Department of Radiation Oncology; Amy M. Ehrlich, Drs. Trina A. Knotts and Michael L. Goodson from the Raybould lab; Drs. Douglas Rowland, Abhijit Chaudhari and Zacchary Harmany from the UC Davis CMGI; Matt Rolston from UC Davis Host Microbe Systems Biology Core, and Dr. Qian Chen in the UC Davis Pathology Core for their technical expertise and help. Editorial services were provided by Nancy R. Gough (BioSerendipity, LLC, Elkridge, MD).

FUNDING

This was work funded by NIH grants R01 CA214048, R01 HL056067, R37 AI034495, P01 CA039542, the UC Davis Comprehensive Cancer Center Support Grant (CCSG) (P30 CA093373) and the UC Davis Mouse Metabolic Phenotyping Center (MMPC) grant (DK092993). The content of this publication does not necessarily reflect the view or policies of the Department of Health and Human Services, nor does mention of trade names, commercial products or organizations imply endorsement by the US Government.

COMPETING INTERESTS

B.R.B. is an advisory board member for Kadmon Pharmaceuticals, Five Prime Therapeutics (no longer active), Magenta Therapeutics, BlueRock Therapeutics; receives funding from BlueRock Therapeutics; and is a founder of Tmunity. A.M.M. is an advisory board member for Genentech, Astra-Zeneca, BMS, Merck, Zosano, Transgene, Dynavax, Incyte. S.H. has served as a consultant for Incyte, CSL Behring, BMS, and Regeneron. D.K. serves as CEO of CoreBiome, a company involved in the commercialization of gut microbiota analyses that is now a wholly owned subsidiary of OraSure.

REFERENCES

1. Blazar BR, Murphy WJ, Abedi M, Advances in graft-versus-host disease biology and therapy. Nat Rev Immunol 12, 443–458 (2012). [PubMed: 22576252]

2. Flegal KM, Carroll MD, Kit BK, Ogden CL, Prevalence of obesity and trends in the distribution of body mass index among US adults, 1999–2010. JAMA 307, 491–497 (2012). [PubMed: 22253363]
3. Navarro WH et al. , Effect of body mass index on mortality of patients with lymphoma undergoing autologous hematopoietic cell transplantation. Biol Blood Marrow Transplant 12, 541–551 (2006). [PubMed: 16635789]
4. Fuji S et al. , Possible association between obesity and posttransplantation complications including infectious diseases and acute graft-versus-host disease. Biol Blood Marrow Transplant 15, 73–82 (2009). [PubMed: 19135945]
5. Jaime-Perez JC et al. , Obesity is associated with higher overall survival in patients undergoing an outpatient reduced-intensity conditioning hematopoietic stem cell transplant. Blood Cells Mol Dis 51, 61–65 (2013). [PubMed: 23422842]
6. McQuade JL et al. , Association of body-mass index and outcomes in patients with metastatic melanoma treated with targeted therapy, immunotherapy, or chemotherapy: a retrospective, multicohort analysis. Lancet Oncol 19, 310–322 (2018). [PubMed: 29449192]
7. Wang Z et al. , Paradoxical effects of obesity on T cell function during tumor progression and PD-1 checkpoint blockade. Nat Med 25, 141–151 (2019). [PubMed: 30420753]
8. van den Berg SM et al. , Diet-induced obesity in mice diminishes hematopoietic stem and progenitor cells in the bone marrow. FASEB J 30, 1779–1788 (2016). [PubMed: 26813974]
9. Nagareddy PR et al. , Adipose tissue macrophages promote myelopoiesis and monocytosis in obesity. Cell Metab 19, 821–835 (2014). [PubMed: 24807222]
10. Nathan C, Ding A, Nonresolving inflammation. Cell 140, 871–882 (2010). [PubMed: 20303877]
11. Mirsoian A et al. , Adiposity induces lethal cytokine storm after systemic administration of stimulatory immunotherapy regimens in aged mice. J Exp Med 211, 2373–2383 (2014). [PubMed: 25366964]
12. Kaplan JM et al. , Obesity enhances sepsis-induced liver inflammation and injury in mice. Obesity (Silver Spring) 24, 1480–1488 (2016). [PubMed: 27172993]
13. Strandberg L et al. , Mice chronically fed high-fat diet have increased mortality and disturbed immune response in sepsis. PLoS One 4, e7605 (2009). [PubMed: 19865485]
14. Sun K, Li M, Sayers TJ, Welniak LA, Murphy WJ, Differential effects of donor T-cell cytokines on outcome with continuous bortezomib administration after allogeneic bone marrow transplantation. Blood 112, 1522–1529 (2008). [PubMed: 18539902]
15. Hartwell MJ et al. , An early-biomarker algorithm predicts lethal graft-versus-host disease and survival. JCI Insight 2, e89798 (2017). [PubMed: 28194439]
16. Reichenbach DK et al. , The IL-33/ST2 axis augments effector T-cell responses during acute GVHD. Blood 125, 3183–3192 (2015). [PubMed: 25814531]
17. Hamilton BL, L3T4-positive T cells participate in the induction of graft-vs-host disease in response to minor histocompatibility antigens. J Immunol 139, 2511–2515 (1987). [PubMed: 3498761]
18. Schroeder MA, DiPersio JF, Mouse models of graft-versus-host disease: advances and limitations. Dis Model Mech 4, 318–333 (2011). [PubMed: 21558065]
19. Reddy P, Negrin R, Hill GR, Mouse models of bone marrow transplantation. Biol Blood Marrow Transplant 14, 129–135 (2008). [PubMed: 18162233]
20. Korngold R, Sprent J, Variable capacity of L3T4+ T cells to cause lethal graft-versus-host disease across minor histocompatibility barriers in mice. J Exp Med 165, 1552–1564 (1987). [PubMed: 3108446]
21. Zhang Y, Joe G, Hexner E, Zhu J, Emerson SG, Alloreactive memory T cells are responsible for the persistence of graft-versus-host disease. J Immunol 174, 3051–3058 (2005). [PubMed: 15728519]
22. Pai CC et al. , Therapeutic benefit of bortezomib on acute graft-versus-host disease is tissue specific and is associated with interleukin-6 levels. Biol Blood Marrow Transplant 20, 1899–1904 (2014). [PubMed: 25064746]
23. Boudry G et al. , Bovine milk oligosaccharides decrease gut permeability and improve inflammation and microbial dysbiosis in diet-induced obese mice. J Dairy Sci 100, 2471–2481 (2017). [PubMed: 28131576]

24. Hamilton MK et al. , Prebiotic milk oligosaccharides prevent development of obese phenotype, impairment of gut permeability, and microbial dysbiosis in high fat-fed mice. Am J Physiol Gastrointest Liver Physiol 312, G474–G487 (2017). [PubMed: 28280143]
25. Murakami Y, Tanabe S, Suzuki T, High-fat Diet-induced Intestinal Hyperpermeability is Associated with Increased Bile Acids in the Large Intestine of Mice. J Food Sci 81, H216–222 (2016). [PubMed: 26595891]
26. Jenq RR et al. , Regulation of intestinal inflammation by microbiota following allogeneic bone marrow transplantation. J Exp Med 209, 903–911 (2012). [PubMed: 22547653]
27. Mathewson ND et al. , Gut microbiome-derived metabolites modulate intestinal epithelial cell damage and mitigate graft-versus-host disease. Nat Immunol 17, 505–513 (2016). [PubMed: 26998764]
28. Ley RE et al. , Obesity alters gut microbial ecology. Proc Natl Acad Sci U S A 102, 11070–11075 (2005). [PubMed: 16033867]
29. Shono Y et al. , Increased GVHD-related mortality with broad-spectrum antibiotic use after allogeneic hematopoietic stem cell transplantation in human patients and mice. Sci Transl Med 8, 339ra371 (2016).
30. Stein-Thoeringer CK et al. , Lactose drives Enterococcus expansion to promote graft-versus-host disease. Science 366, 1143–1149 (2019). [PubMed: 31780560]
31. Taur Y et al. , The effects of intestinal tract bacterial diversity on mortality following allogeneic hematopoietic stem cell transplantation. Blood 124, 1174–1182 (2014). [PubMed: 24939656]
32. Staffas A, Burgos da Silva M, van den Brink MR, The intestinal microbiota in allogeneic hematopoietic cell transplant and graft-versus-host disease. Blood 129, 927–933 (2017). [PubMed: 27940475]
33. Poglio S et al. , Adipose tissue sensitivity to radiation exposure. Am J Pathol 174, 44–53 (2009). [PubMed: 19095959]
34. Vossen JM et al. , Complete suppression of the gut microbiome prevents acute graft-versus-host disease following allogeneic bone marrow transplantation. PLoS One 9, e105706 (2014). [PubMed: 25180821]
35. Weber D et al. , Rifaximin preserves intestinal microbiota balance in patients undergoing allogeneic stem cell transplantation. Bone Marrow Transplant 51, 1087–1092 (2016). [PubMed: 26999466]
36. van Bekkum DW, Knaan S, Role of bacterial microflora in development of intestinal lesions from graft-versus-host reaction. J Natl Cancer Inst 58, 787–790 (1977). [PubMed: 14265]
37. O'Toole PW, Jeffery IB, Gut microbiota and aging. Science 350, 1214–1215 (2015). [PubMed: 26785481]
38. Pagliardini T et al. , Post-transplantation cyclophosphamide-based haploidentical versus Atg-based unrelated donor allogeneic stem cell transplantation for patients younger than 60 years with hematological malignancies: a single-center experience of 209 patients. Bone Marrow Transplant 54, 1067–1076 (2019). [PubMed: 30401970]
39. Sikder K, Shukla SK, Patel N, Singh H, Rafiq K, High Fat Diet Upregulates Fatty Acid Oxidation and Ketogenesis via Intervention of PPAR-gamma. Cell Physiol Biochem 48, 1317–1331 (2018). [PubMed: 30048968]
40. Byersdorfer CA et al. , Effector T cells require fatty acid metabolism during murine graft-versus-host disease. Blood 122, 3230–3237 (2013). [PubMed: 24046012]
41. Lerner KG et al. , Histopathology of graft-vs.-host reaction (GvHR) in human recipients of marrow from HL-A-matched sibling donors. Transplant Proc 6, 367–371 (1974). [PubMed: 4155153]
42. Amin K et al. , Amphiregulin in intestinal acute graft-versus-host disease: a possible diagnostic and prognostic aid. Mod Pathol 32, 560–567 (2019). [PubMed: 30425334]
43. Cooke KR et al. , An experimental model of idiopathic pneumonia syndrome after bone marrow transplantation: I. The roles of minor H antigens and endotoxin. Blood 88, 3230–3239 (1996). [PubMed: 8963063]
44. Pai CS, Khuat LT, Chen M, Murphy WJ, Abedi M, Therapeutic Effects of a NEDD8-Activating Enzyme Inhibitor, Pevonedistat, on Sclerodermatous Graft-versus-Host Disease in Mice. Biol Blood Marrow Transplant 23, 30–37 (2017). [PubMed: 27815049]

45. Segata N et al. , Metagenomic biomarker discovery and explanation. Genome Biol 12, R60 (2011). [PubMed: 21702898]

46. Al-Ghalith GA, Hillmann B, Ang K, Shields-Cutler R, Knights D, SHI7 Is a Self-Learning Pipeline for Multipurpose Short-Read DNA Quality Control. mSystems 3, (2018).

47. Vangay P et al. , US Immigration Westernizes the Human Gut Microbiome. Cell 175, 962–972 e910 (2018). [PubMed: 30388453]

48. Pai CC et al. , Treatment of chronic graft-versus-host disease with bortezomib. Blood 124, 1677–1688 (2014). [PubMed: 25009225]

49. Zhang Y, Louboutin JP, Zhu J, Rivera AJ, Emerson SG, Preterminal host dendritic cells in irradiated mice prime CD8+ T cell-mediated acute graft-versus-host disease. J Clin Invest 109, 1335–1344 (2002). [PubMed: 12021249]

50. Tawara I et al. , Interleukin-6 modulates graft-versus-host responses after experimental allogeneic bone marrow transplantation. Clin Cancer Res 17, 77–88 (2011). [PubMed: 21047980]

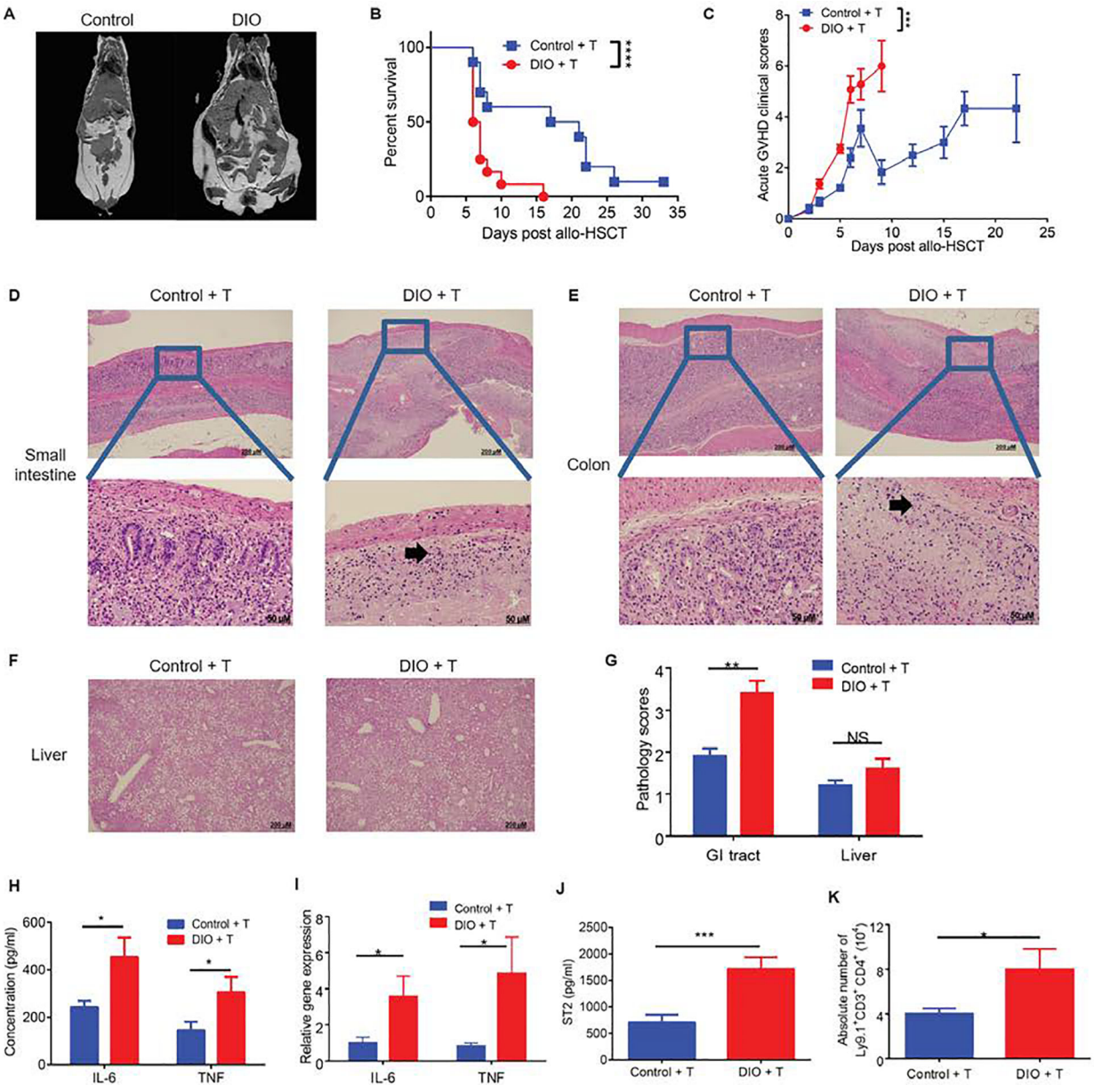

Figure 1. Obesity accelerates acute GVHD in a major mismatched mouse model.

C57BL/6 male mice ($H2^b$) received total body irradiation (TBI) (1050 cGy) and T cell-depleted bone marrow (BM) cells with or without purified T cells ($4.5 – 9 \times 10^6$) from donor BALB/c mice ($H2^d$). Control + T, control mice transplanted with BM and T cells; DIO + T, DIO mice transplanted with BM and T cells. **(A)** Magnetic resonance images (MRI) of nontransplant control and DIO C57BL/6 mice. **(B)** Survival rates (n = 10–12 mice/group) displayed as Kaplan-Meier curves analyzed by a log-rank test. **(C)** Acute GVHD (aGVHD) clinical scores (n = 10–12 mice/group). Statistical significance was determined by two-way analysis of variance (ANOVA) with Tukey's post hoc test for comparison among groups. **(D-F)** Hematoxylin and eosin (H&E) staining of small intestine samples, colon samples, and liver samples at day 6 post allo-HSCT. Black arrows indicates mucosal necrosis. Scale bars: 200μm, 50μm. **(G)** Pathology scores for GI tract and liver at day 6 post allo-HSCT

(n = 5 mice/group). **(H)** Serum IL-6 and TNF concentrations at day 6 post allo-HSCT (n = 6–7 mice/group). **(I)** Relative expression of the genes encoding IL-6 and TNF in the small intestine at day 6 post allo-HSCT (n = 7– 8 mice/group). **(J)** Serum ST2 concentration at day 6 post allo-HSCT (n = 4 mice/group). **(K)** Number of donor $CD4^+$ T cells in the mesenteric lymph nodes at day 8 post allo-HSCT (n = 4 mice/group). Bar graphs depict mean ± standard error of mean (s.e.m). Each experiment was performed at least twice. In panel G – K, nonparametric Mann-Whitney test was used to compare two unpaired groups. *p < 0.05, **p < 0.01, ***p < 0.001, ****p < 0.0001, ns, not significant.

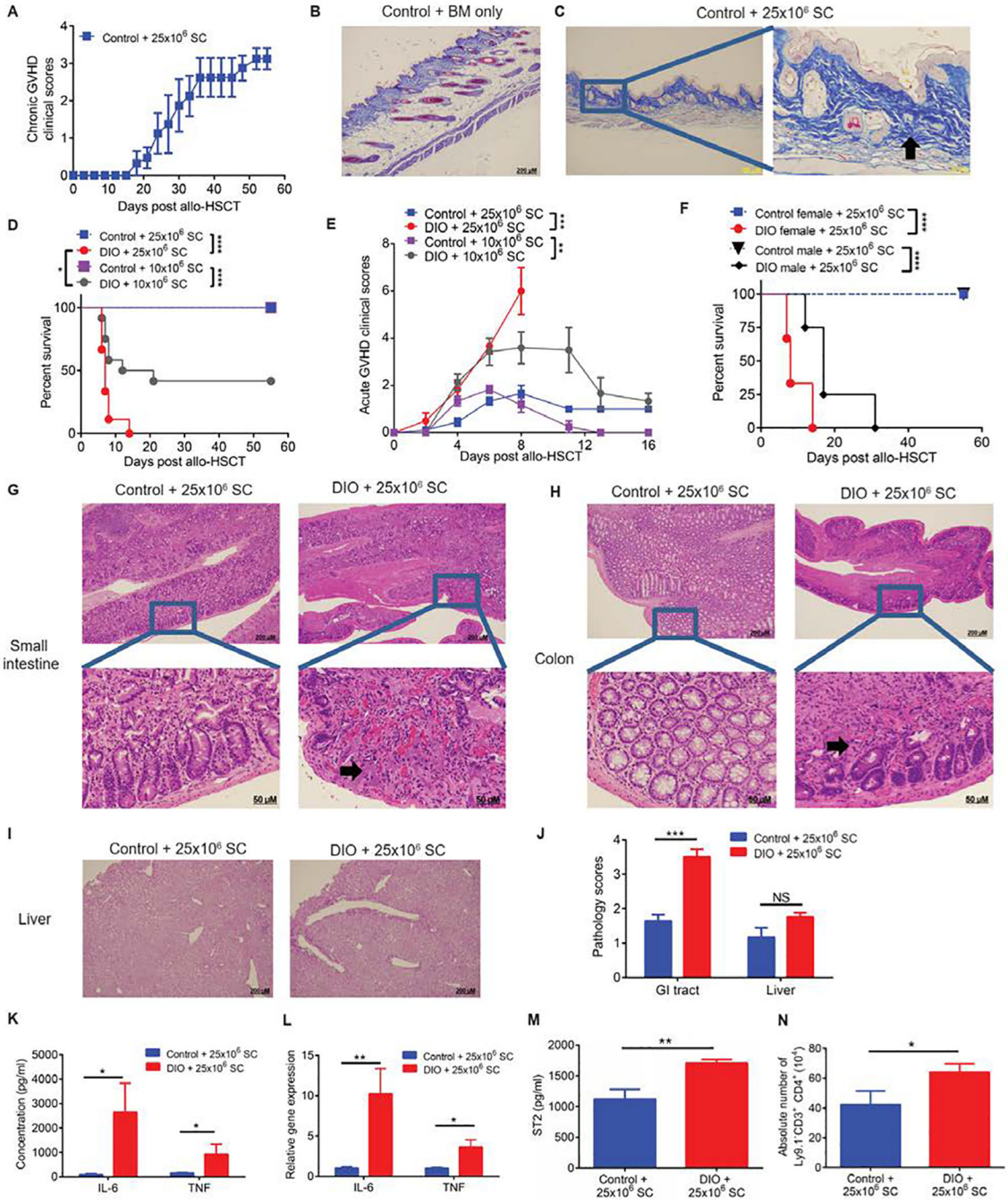

Figure 2. Obesity induces GI tract acute GVHD in a mouse model of sclerodermatous chronic GVHD.

Lean (control) or obese (DIO) female BALB/c mice ($H2^d$) received total body irradiation (TBI) 800 cGy and underwent transplantation with bone marrow (BM) cells with or without splenocytes (10–25 × 10^6) from donor B10.D2 ($H2^d$) mice. Control mice were a healthy weight. BM only, recipient of bone marrow cells without splenocytes; 25M SC, recipient of bone marrow cells + 25 × 10^6 splenocytes; 10M SC, recipient of bone marrow cells + 10 × 10^6 splenocytes. **(A)** Chronic GVHD (cGVHD) score of control mice with sclerodermatous

GVHD. (**B, C**) Representative images of trichrome staining of the skin from control mice transplanted with bone marrow cells only and control mice transplanted with bone marrow cells + splenocytes showing evidence of sclerodermatous cGVHD. Tissues were from mice at day 55 post allo-HSCT. Black arrow indicates collagen deposition. Scale bars, 200μm or 50μm. **(D)** Survival rates of control and DIO mice receiving 10×10^6 or 25×10^6 splenocytes, shown as Kaplan-Meier curves (n = 9–12 mice/group). **(E)** Acute GVHD (aGVHD) clinical scores (n = 9 −12 mice/group). **(F)** Survival rates of control and DIO mice of different sexes (n = 4 mice/group), shown as Kaplan-Meier curves. **(G-I)** Hematoxylin and eosin (H&E) staining of small intestine samples, colon samples, and liver samples at day 6 post allo-HSCT. Black arrows indicate the destruction of crypt structures in the gut. Scale bars, 200μm or 50μm. **(J)** Pathology scores for GI tract and liver at day 6 post allo-HSCT (n = 6–8 mice/group). **(K)** Serum IL-6 and TNF concentrations at day 6 post allo-HSCT (n = 6 mice/group). **(L)** Relative expression of genes encoding IL-6 and TNF in the small intestine at day 6 post allo-HSCT (n = 5–6 mice/group). **(M)** Serum ST2 concentrations at day 6 post allo-HSCT (n = 6–7 mice/group). **(N)** Number of donor $CD4^+$ T cells in the mesenteric lymph nodes at day 7 post allo-HSCT (n = 7 mice/group). Bar graphs depict mean ± s.e.m. Each experiment was performed at least twice. In D and F, Kaplan-Meier survival curves were analyzed by a log-rank test. In E, clinical scores were analyzed by 2-way analysis of variance (ANOVA) with Tukey's post hoc test for comparison among groups. In panels J and K, nonparametric Mann-Whitney tests were used to compare two unpaired groups. *p < 0.05, **p < 0.01, ***p < 0.001, ****p < 0.0001.

A University of Minnesota

BMI	# patient	Age	Relationship with donors	Conditioning	Disease
< 30	22	18-70	Unrelated	Non-myeloblative (13), Full preparation (9)	Acute myeloid leukemia (10), Acute lymphoid leukemia (2), Myelodysplastic Syndromes (4), non-Hodgkin lymphoma (2), others (4)
> 30	15	31-71	Unrelated	Non-myeloblative (8), Full preparation (7)	Acute myeloid leukemia (6), Acute lymphoid leukemia (3), Myelodysplastic Syndromes (3), Chronic myeloid leukemia (2), B-cell/Small lymphocytic lymphoma (1)

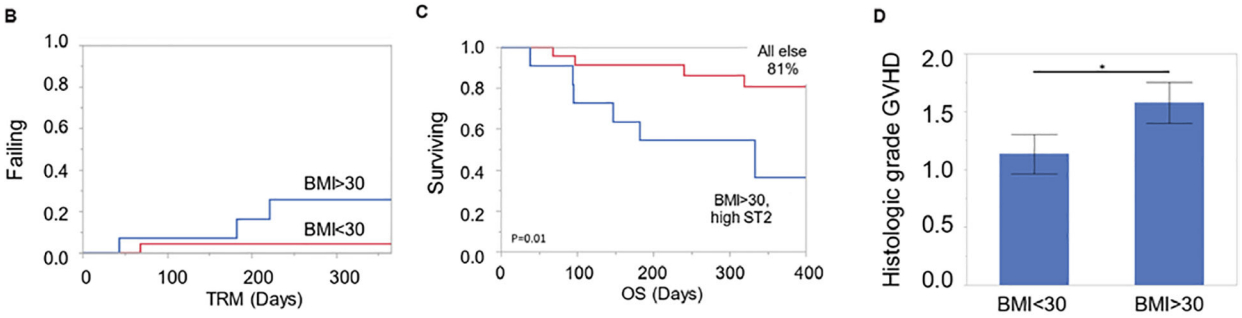

E The Tisch Cancer Institute at Mount Sinai

BMI	# patient	Age	Relationship with donors	Disease
< 30	5	23-71	Unrelated mismatched (5)	Acute leukemia (4), Multiple myeloma (1)
> 30	5	40-63	Unrelated mismatched (4), Related mismatched (1)	Acute leukemia (2), Myelodysplastic Syndromes (1), Multiple myeloma (1), other leukemia (1)

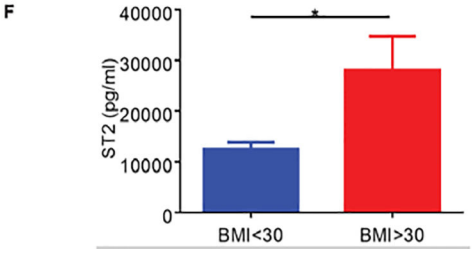

Figure 3. Obesity correlates with lower survival rate after mismatched allo-HSCT in human patients.

(A) Patient characteristics from one cohort at University of Minnesota stratified by BMI above or below 30. The numbers of patients with each characteristic are indicated in parentheses. **(B)** Shown is transplant-related mortality (TRM) in the days after mismatched allo-HSCT for the cohort described in A. **(C)** Shown is survival outcome for patients after allo-HSCT; 11 of 37 patients had a BMI > 30 and high ST2 serum concentrations. Kaplan-Meier survival curves were analyzed by a log-rank test. **(D)** Pathology scores for intestinal biopsies of patients in the cohort described in A are. shown. Statistical significance was analyzed by nonparametric Mann-Whitney test. **(E)** Patient characteristics for the cohort from the Tisch Cancer Institute stratified by BMI are shown. **(F)** Shown are serum ST2 concentrations at day 7 post allo-HSCT for the 10 patients described in panel E. Statistical significance was analyzed by nonparametric Mann-Whitney test. *$p < 0.05$.

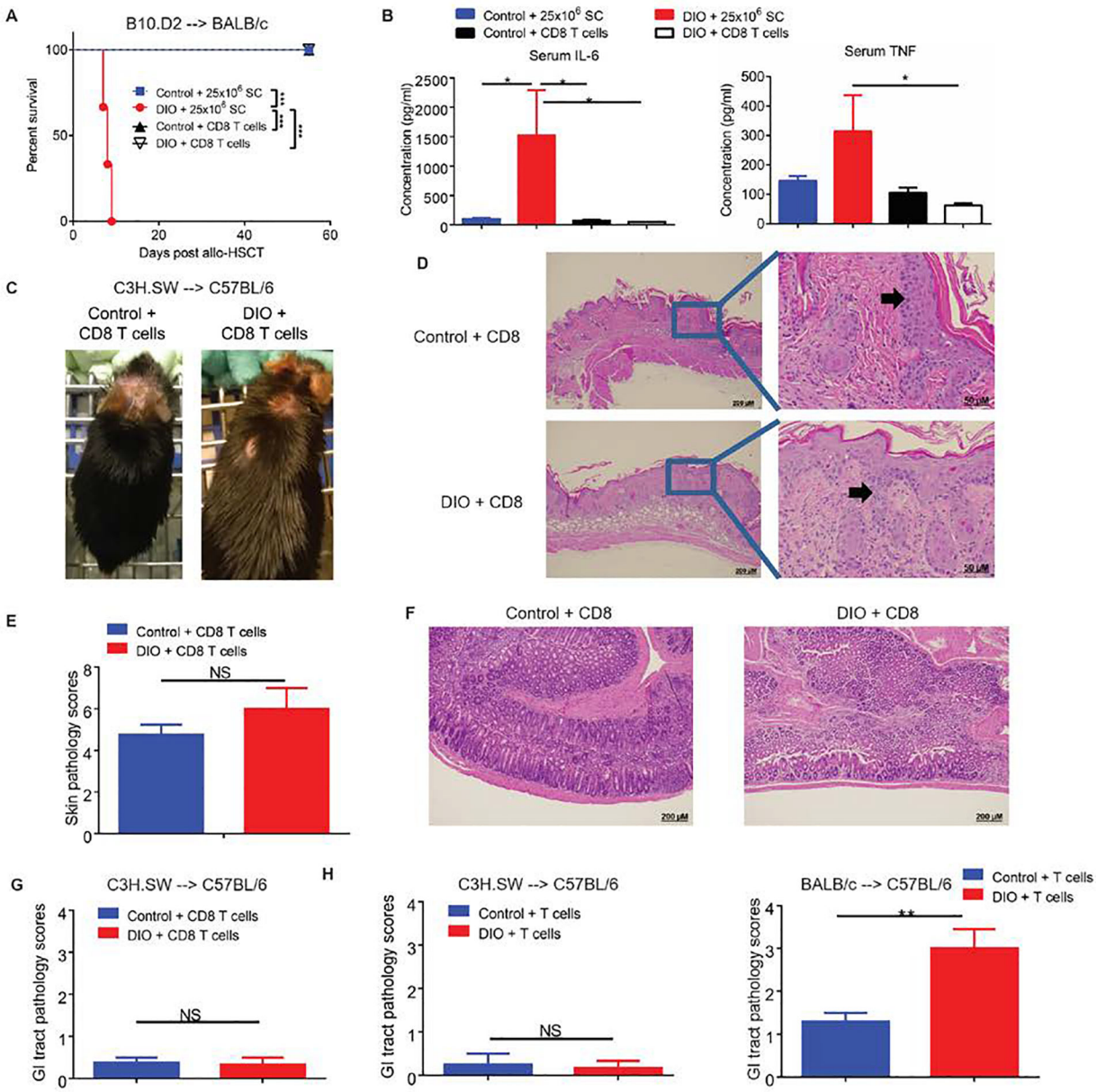

Figure 4. Acute GVHD in obese mouse recipients is mediated by donor CD4$^+$ T cells.

(A, B) Female BALB/c lean (control) and obese (DIO) mice received total body irradiation (TBI) 800 cGy and underwent transplantation with bone marrow (BM) cells and with either whole splenocytes (SC) or purified CD8$^+$ T cells from B10.D2 mice. Shown are survival rates (A) and serum IL-6 and TNF concentrations at day 6 post allo-HSCT (B) (n = 3–4 mice/group). Kaplan-Meier survival curves were analyzed by a log-rank test. **(C-H)** Female lean (control) and obese (DIO) C57BL/6 mice (H2^b) received TBI (1050 cGy) and T cell-depleted bone marrow cells with either purified T cells or purified CD8$^+$ T cells (3×10^6) from C3H.SW (H2^b) mice. (**C**) Representative images of control and DIO mice developing skin GVHD at day 33 post allo-HSCT. (**D**) Hematoxylin and eosin (H&E) staining of skin samples from control and DIO mice transplanted with purified CD8$^+$ T cells at day 36 post allo-HSCT. Black arrows indicate inflammatory cell infiltration. Scale

bar, 200μm. (E) Pathology scores of skin samples from control and DIO mice transplanted with purified $CD8^+$ T cells at day 36 post allo-HSCT (n = 5 – 6 mice/group). (F) H&E staining of GI tract samples from control and DIO mice transplanted with purified $CD8^+$ T cells at day 36 post allo-HSCT. Scale bar, 200μm. (G) Pathology scores of GI tract samples from control and DIO mice transplanted with purified $CD8^+$ T cells at day 36 post allo-HSCT (n = 3–4 mice/group). (H) Comparison of pathology scores of GI tract samples for $CD8^+$ T cell-dependent minor MHC mismatch model (C3H.SW into C57BL/6) and $CD4^+$ T cell-dependent major MHC mismatch model (BALB/c into C57BL/6) (n = 3 – 5 mice/group). Bar graphs depict mean ± s.e.m. Each experiment was performed at least twice. In B, E, G, and H, nonparametric Mann-Whitney test was used to compare two unpaired groups. *$p < 0.05$, **$p < 0.01$, ***$p<0.001$, ns, not significant.

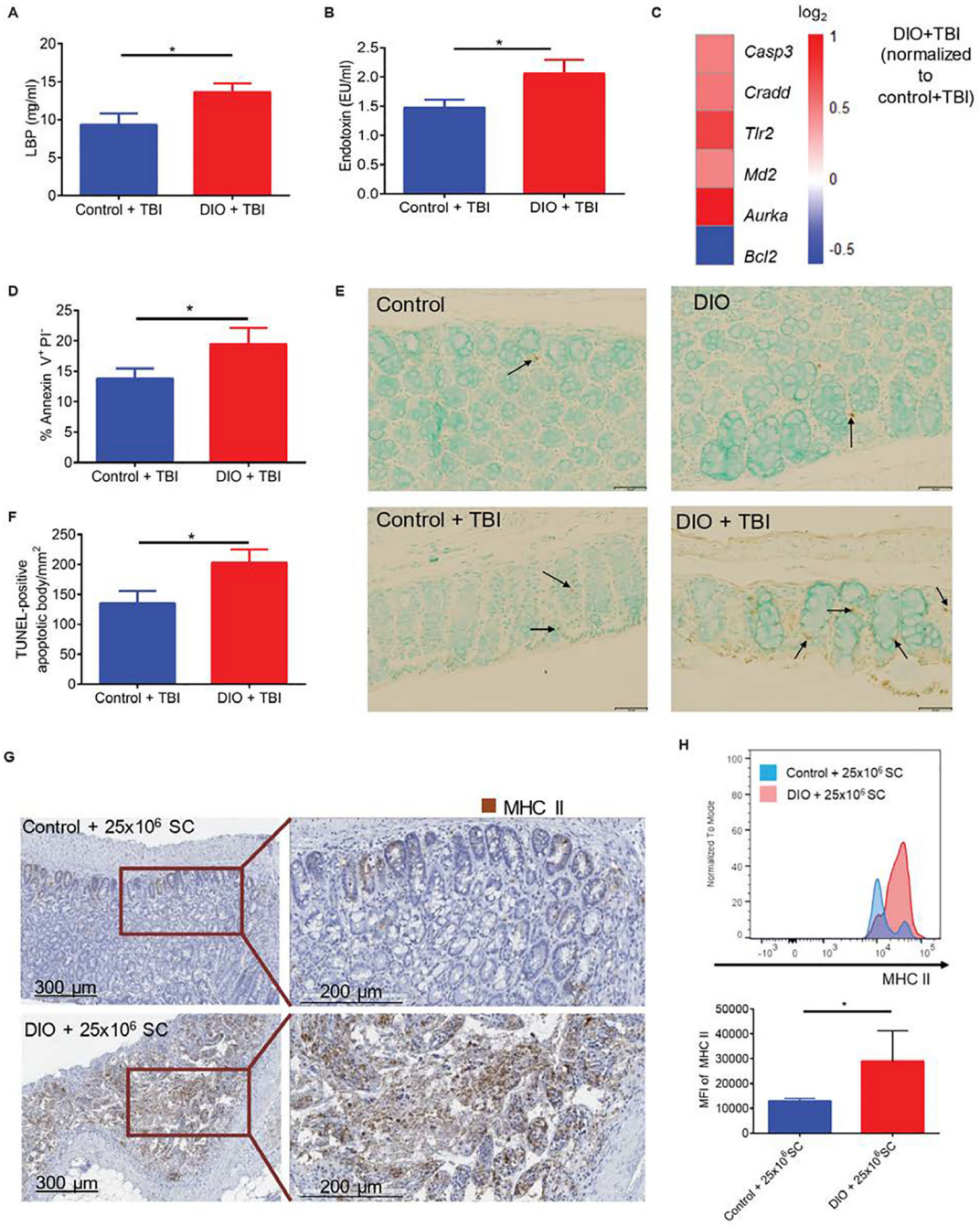

Figure 5. Increased intestinal permeability and apoptosis in obese mice after irradiation.

(A-F) Control lean and obese DIO BALB/c mice received 800 cGy of total body irradiation (TBI). (**A**) LPS-binding protein (LBP) serum concentrations for control and DIO mice at day 2 post-irradiation (7–8 mice/group). (**B**) Endotoxin serum concentrations for control and DIO mice at day 2 post-irradiation (3 mice/group). (**C**) Relative gene expression at day 2 post-irradiation (normalized to control mice + 800 cGy). (**D**) Percentage of Annexin V^+ PI^- cells in the intestine at day 2 post-irradiation (n = 7–8 mice/group). (**E**) Representative images of TUNEL-positive cells in the colon of nonirradiated control and DIO mice, and

irradiated control and DIO mice. Black arrows indicate apoptotic cells revealed by TUNEL staining. Scale bar, 50μm. (**F**) Quantification of TUNEL-positive apoptotic bodies/mm^2 in control and DIO mice at day 2 post-irradiation (4 mice/group). **(G)** Representative immunohistochemical images of MHC II abundance in the intestine of control and DIO BALB/c mice transplanted with B10.D2 mouse bone marrow (BM) + splenocytes at day 6 post allo-HSCT. Scale bars, 300μm (left) and 200μm (right). (H) Representative histogram and quantification of mean fluorescence intensity (MFI) of the MHC II^+ cell population gated on $CD45^+$ $CD19^-$ $CD11c^+$ cells in the mesenteric lymph nodes at day 4 post allo-HSCT (n = 3–4 mice/group). Bar graphs depict mean ± s.e.m. Each experiment was performed at least twice. Nonparametric Mann-Whitney tests were used to compare two unpaired groups. *$p < 0.05$.

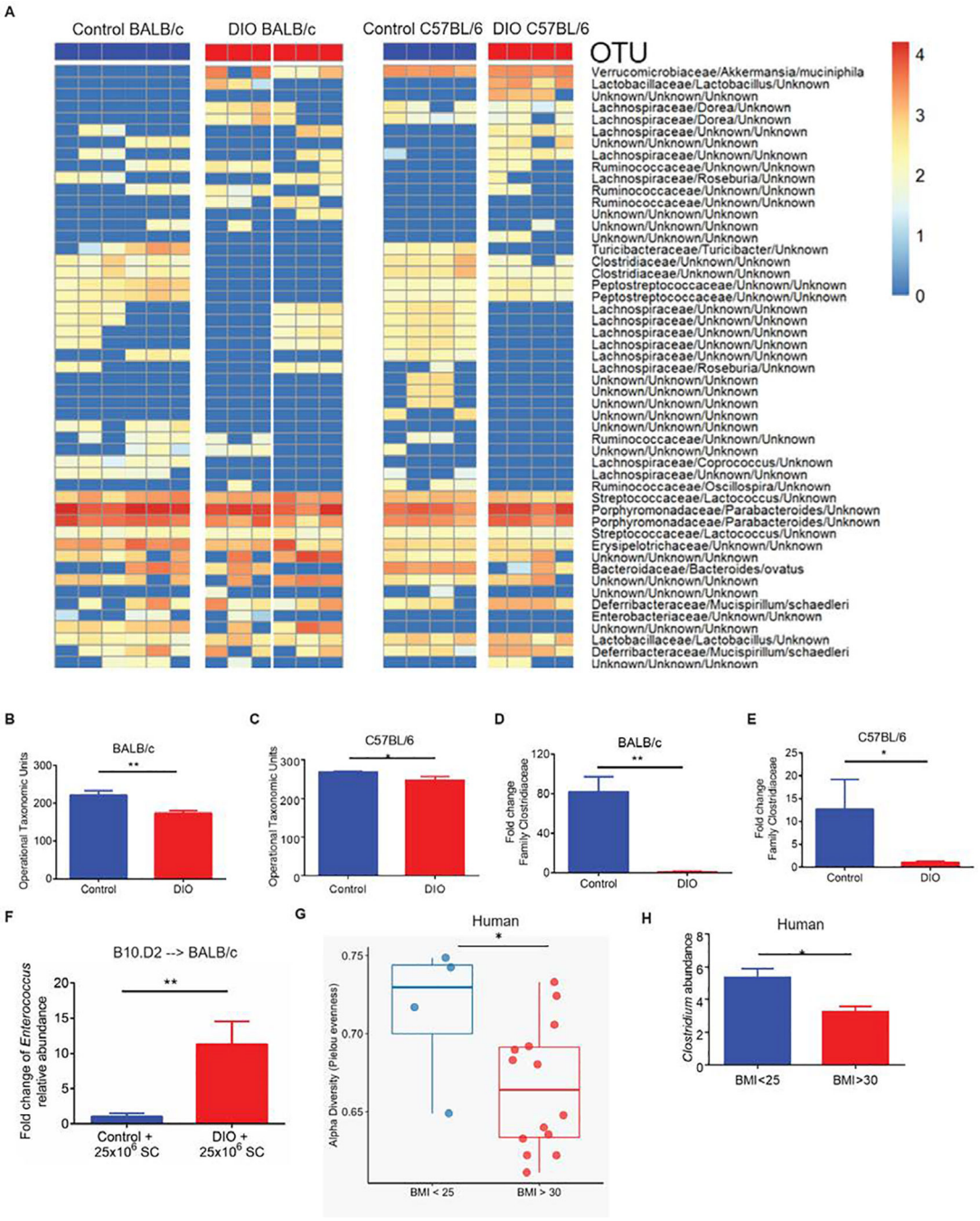

Figure 6. Obesity correlates with restricted gut microbiota diversity and GVHD-associated bacterial taxa.

(A) Taxonomic profiles of fecal samples from nonirradiated control and DIO C57BL/6 mice (n = 4 mice/group) and nonirradiated control and DIO BALB/c (n = 6 mice/group). Each row represents an operational taxonomic unit (OTU). **(B)** Operational taxonomic units in control and DIO BALB/c mice. **(C)** Operational taxonomic units in control and DIO C57BL/6 mice. **(D)** Fold change in family Clostridiaceae for control and DIO BALB/c mice. **(E)** Fold change in family Clostridiaceae for control and DIO C57BL/6 mice (n =

5–6 mice/group). **(F)** Fold change in *Enterococcus* abundance in control and DIO BALB/c mice at day 4 post allo-HSCT (B10.D2→BALB/c + SC model, n = 7 – 8 mice/group). **(G)** Gut microbiota α-diversity for patients in the University of Minnesota cohort with a BMI<25 (n=4) or a BMI>30 (n=14) before allo-HSCT, shown by Pielou's evenness index. **(H)** Abundance of *Clostridium* in lean and obese patients in the University of Minnesota cohort before allo-HSCT. Nonparametric Mann-Whitney tests were used to compare two unpaired groups. *$p < 0.05$, **$p < 0.01$.

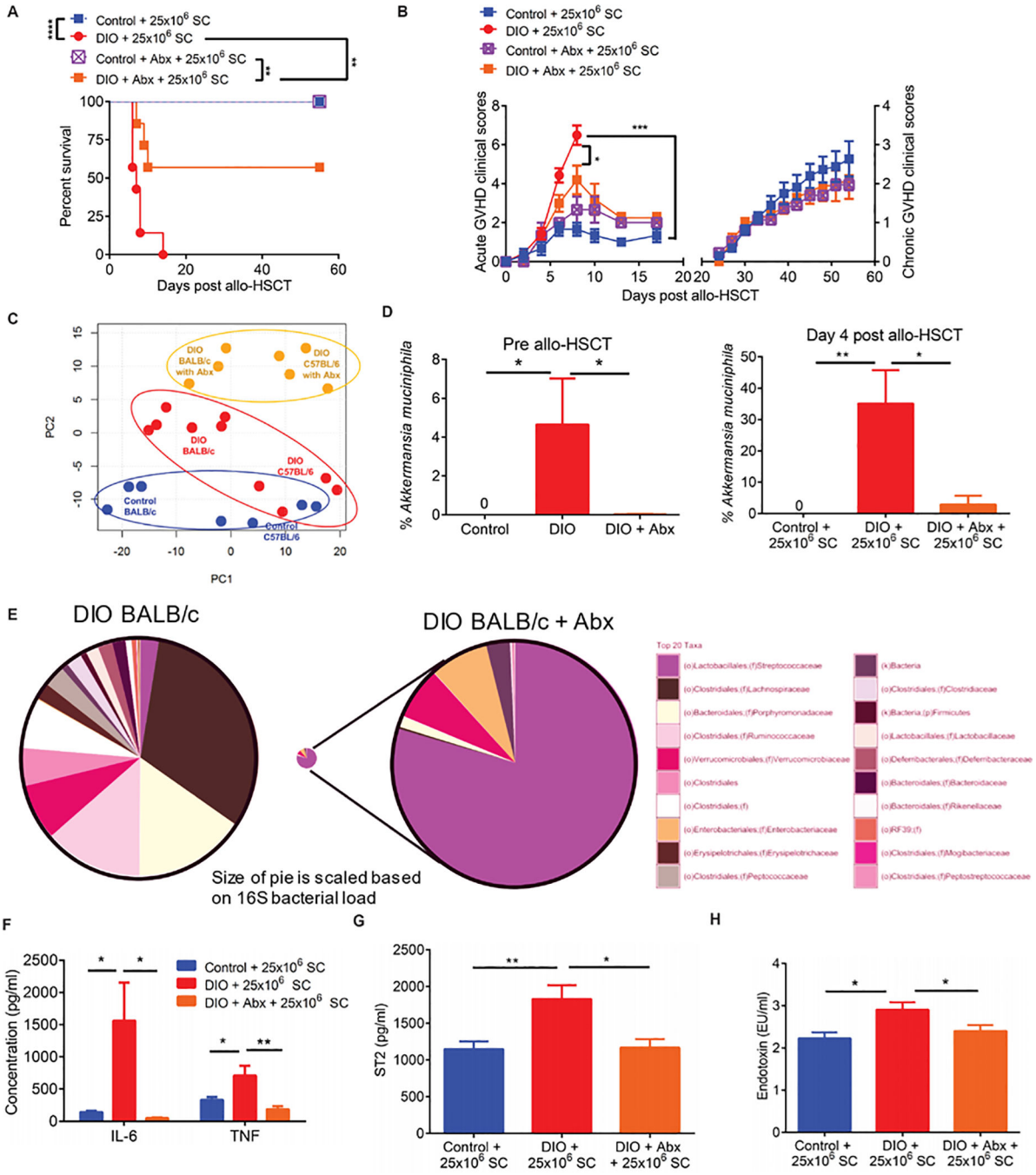

Figure 7. Antibiotic administration before transplant ameliorates acute GVHD in obese recipients.

BALB/c mouse recipients were transplanted with bone marrow (BM) cells and 25 × 10^6 splenocytes from B10.D2 donor mice. Where indicated, the antibiotics (Abx) ampicillin, neomycin, and vancomycin (0.5 mg/ml) were added to drinking water for 14 days before allo-HSCT. **(A)** Kaplan-Meier survival curves after allo-HSCT were analyzed by a log-rank test (n = 7 mice/group). **(B)** aGVHD and cGVHD clinical scores are shown (n = 7 mice/group). Data were analyzed by 2-way analysis of variance (ANOVA) with Tukey's

post hoc test for comparison among groups. **(C)** Principal component (PC) analysis of weighted and normalized UniFrac distances of fecal microbiota from control, DIO, and antibiotic-treated DIO mice. **(D)** Relative abundance of *Akkermansia muciniphila* in fecal samples of control, DIO, and antibiotic-treated DIO BALB/c mice before allo-HSCT and at day 4 after allo-HSCT (n = 3–6 mice/group). **(E)** Bacterial load comparison and bacterial taxa of fecal microbiota from untreated DIO and antibiotic-treated DIO BALB/c mice. Chart for antibiotic-treated mice is shown to scale and enlarged. **(F)** Serum IL-6 and TNF concentrations at day 6 post allo-HSCT (n = 5–7 mice/ group). **(G)** Serum ST2 concentrations at day 6 post allo-HSCT (n = 6–8 mice/group). **(H)** Endotoxin serum concentrations at day 4 post allo-HSCT (n = 6–8 mice/group). Bar graphs depict mean ± s.e.m. Each experiment was performed at least twice. In D, F, G, and H, nonparametric Mann-Whitney tests were used to compare two unpaired groups. *$p < 0.05$, **$p < 0.01$, ***$p < 0.001$, ****$p < 0.0001$.

Table 1.

Mouse models of allo-HSCT.

Recipient mice received a conditioning regimen (total body irradiation) prior to transplant. Donor mice were lean; recipient mice were lean (control) or obese (DIO). BM, bone marrow.

Model	Recipient	Donor	MHC incompatibility	Transplanted cells	Published GVHD model
BALB/c → C57BL/6 + T	C57BL/6	BALB/c	Major	BM + T cells	Acute, GI, liver and skin, lethal (14, 16)
B10.D2 → BALB/c + SC	BALB/c	B10.D2	Minor	BM + splenocytes	Chronic, sclerodermatous (44, 48)
B10.D2 → BALB/c + CD8	BALB/c	B10.D2	Minor	BM + $CD8^+$ T cells	B10.D2BALB/c is CD4-dependent. CD8 T cells are not the cause of GVHD in this strain combination.
B10.D2 → BALB/c + CD4	BALB/c	B10.D2	Minor	BM + $CD4^+$ T cells	Chronic, sclerodermatous (19)
C3H.SW → C57BL/6 + CD8	C57BL/6	C3H.SW	Minor	BM + $CD8^+$ T cells	Acute, skin and liver (22, 49)
C3H.SW → C57BL/6 + T	C57BL/6	C3H.SW	Minor	BM + T cells	(50)